JOURNAL OF GEOPHYSICAL RESEARCH: OCEANS, VOL. 118, 2685–2701, doi:10.1002/jgrc.20207, 2013

Impact of current-wave interaction on storm surge simulation: A case study for Hurricane Bob

Yunfang Sun,[1] Changsheng Chen,[1,2] Robert C. Beardsley,[3] Qichun Xu,[1]
Jianhua Qi,[1] and Huichan Lin[1,2]

Received 2 January 2013; revised 5 April 2013; accepted 18 April 2013; published 30 May 2013.

[1] Hurricane Bob moved up the U.S. east coast and crossed over southern New England and the Gulf of Maine [with peak marine winds up to 54 m/s (100 mph)] on 19–20 August 1991, causing significant damage along the coast and shelf. A 3-D fully wave-current-coupled finite-volume community ocean model system was developed and applied to simulate and examine the coastal ocean responses to Hurricane Bob. Results from process study-oriented experiments showed that the impact of wave-current interaction on surge elevation varied in space and time, more significant over the shelf than inside the inner bays. While sea level change along the coast was mainly driven by the water flux controlled by barotropic dynamics and the vertically integrated highest water transports were essentially the same for cases with and without water stratification, the hurricane-induced wave-current interaction could generate strong vertical current shear in the stratified areas, leading to a strong offshore transport near the bottom and vertical turbulent mixing over the continental shelf. Stratification could also result in a significant difference of water currents around islands where the water is not vertically well mixed.

Citation: Sun, Y., C. Chen, R. C. Beardsley, Q. Xu, J. Qi, and H. Lin (2013), Impact of current-wave interaction on storm surge simulation: A case study for Hurricane Bob, *J. Geophys. Res. Oceans*, *118*, 2685–2701, doi:10.1002/jgrc.20207.

1. Introduction

[2] In addition to nor'easters (extra-tropical cyclones), hurricanes (tropic cyclones) have also caused significant damage in the New England coastal region. The national oceanic and atmospheric administration (NOAA) hurricane database (http://www.csc.noaa.gov/hurricanes/) reports that since the start of record keeping in 1851, a total of 55 hurricanes have swept the southern New England coastal region (defined here as a 400-km diameter circular region centered at 70.97°W, 41.55°N; Figure 1). Classified using the Saffir-Simpson hurricane scale, one were category 5 (H5), four H4, 19 H3, 12 H2, and 19 H1 hurricanes. In this group, only 21 hurricanes retained hurricane strength after reaching this region.

[3] Hurricane Bob originally appeared as a low-pressure area in the Atlantic Ocean near the Bahamas (74.3°W, 25.6°N) at 00:00 GMT on 16 August 1991. The depression steadily intensified and became a tropical storm 18 h later. The storm continued to strengthen as it moved northwestward and became "Hurricane Bob" at 77.10°W, 29.00°N at 18:00 GMT on 17 August 1991. Hurricane Bob initially moved northeastward and brushed the North Carolina shelf between 18:00 GMT on 18 August 1991 through 00:00 GMT on 19 August 1991, during which it reached H3 with maximum sustained winds of 51.4 m/s. Around 18:00 GMT on 19 August 1991, Hurricane Bob had weakened to H2 and made landfall near Newport, Rhode Island (Figure 1). Shortly thereafter, it rapidly deteriorated to a tropical storm and moved across the Gulf of Maine (GoM) toward Maine and Canada, dissipating finally west of Portugal on 29 August 1991 after a long transit across the North Atlantic Ocean. The strong winds (>40 m/s), high storm surge, and heavy rains produced by Hurricane Bob caused extensive damage over New England with a total loss of $1.5 billion in economy, cleanup costs, uninsured losses, and flood claims [*Mayfield*, 1992]. This huge loss was due to the passage of the storm over a densely populated region, although Hurricane Bob was only a H2 hurricane when it landed.

[4] In the last decade, especially following Hurricane Katrina in 2005, hurricane-induced storm surge and coastal inundation have received intense attention in the United States. Advances in the development of unstructured grid ocean models in recent years have made it practical to accurately resolve the coastal geometry: a prerequisite for a model to simulate surges and inundation. Examples can be seen in hurricane simulations done in the Gulf of Mexico by *Westerink et al*. [2008] using ADvanced CIRCulation Model and *Weisberg and Zheng* [2006, 2008], *Rego and Li* [2010a, 2010b], and *Dukhovskoy and Morey*

[1]School for Marine Science and Technology, University of Massachusetts Dartmouth, New Bedford, Massachusetts, USA.
[2]International Center for Marine Studies, Shanghai Ocean University, Shanghai, China.
[3]Department of Physical Oceanography, Woods Hole Oceanographic Institution, Woods Hole, Massachusetts, USA.

Corresponding author: Y. Sun, School for Marine Science and Technology, University of Massachusetts Dartmouth, 706 South Rodney French Blvd., New Bedford, MA 02744, USA. (yf.sun@umassd.edu)

©2013. American Geophysical Union. All Rights Reserved.
2169-9275/13/10.1002/jgrc.20207

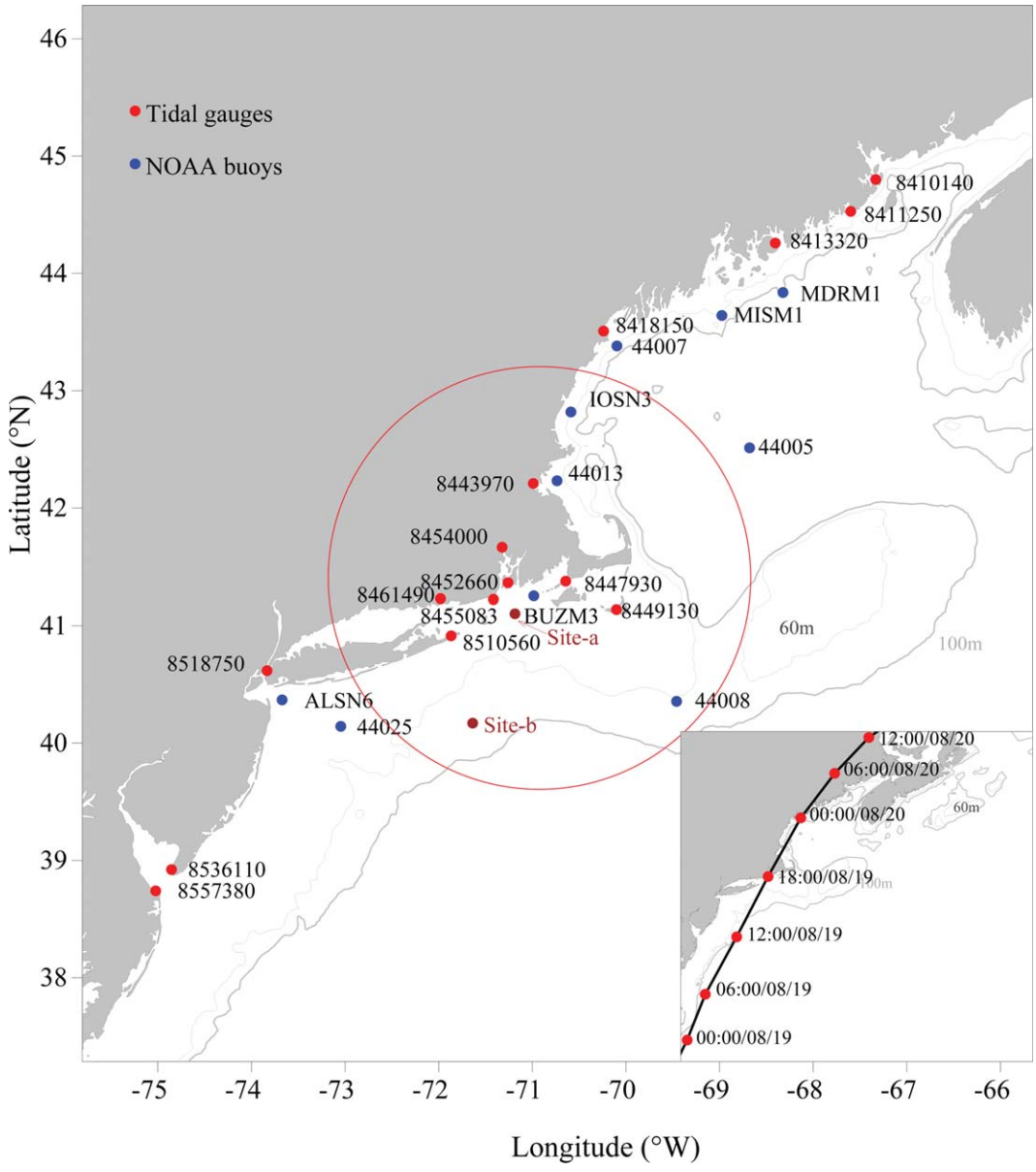

Figure 1. Locations of coastal buoys and tidal gauges in the computational domain for Hurricane Bob-induced storm surge simulation. Red dots represent tidal gauges, and blue dots represent NOAA buoys. Orange dots represent sites selected to display vertical profiles of water temperature and velocity. The subfigure in the right-lower corner shows the path of Hurricane Bob from 00:00 GMT 19 August 1991 to 12:00 GMT 20 August 1991.

[2011] using finite-volume community ocean model (FVCOM). *Chen et al*. [2008] examined the impact of coastal geometric fitting on inundation in an estuary through comparison between unstructured and structured grid models. They pointed out that failure to resolve local geometry in a complex coastal system in a structured grid-based model could lead to poor simulation of water exchange processes in the inundation zone.

[5] The recent development of unstructured grid surface wave models has made it possible to use a fully coupled wave-current model for storm surge simulation. However, the high computational cost has raised a question if this is really necessary, especially when using the system for forecasting. It is clear that storm-driven surface waves is one of the key processes that cause "splash-over" or overtopping of coastal barriers (e.g., seawalls) [*McCoy et al*., 2008; *Kees et al*., 2011] and morphologic changes of the seafloor due to sediment transport [*Morton*, 2008]; however, it is unclear whether or not wave-current interaction causes a significant change in the surge level. Seawater is generally treated as an incompressible fluid, in which sea level change is caused by the divergence-convergence of water transport. In a fully coupled wave-current model, surface waves contribute to water level through changes in the horizontal momentum due to radiation stress and bottom friction. A question here is that under what conditions could

these two processes cause large changes in the net water transport toward the coast? In many coastal regions, the near-shore water depth is generally in order of a few meters. When a hurricane passes over these regions, the water becomes vertically well mixed. In the coastal inlets or bays, however, the water could be stratified, particularly during the summer season. Even during the hurricane passage, the water column might not become vertically well mixed. In such situations, a hurricane could cause a large water transport in the surface mixed layer and a return flow in the underlying stratified layer. How does the vertical stratification affect the water transport toward the coast? How do such processes change with inclusion of wave-current interaction? To our knowledge, these questions have not been well explored for hurricane-induced surge simulation in the northeast United States. *Cheung et al*. [2007] applied a fully wave-current structured grid model to simulate Hurricane Bob-induced surges. Their use of a barotropic model precluded addressing the above questions.

[6] This paper presents our findings on the roles surface waves play in determining water level and transport in hurricane-induced storm surge simulation. Studies were carried out using the fully coupled wave-current version of FVCOM (3.1.6) within the framework of the Northeast Coastal Ocean Forecast System (NECOFS), through which simulations were made under realistic ocean conditions including stratification. The paper is organized as follows. In section 2, the coupled model and numerical experiments are described. In section 3, the simulation results with and without inclusion of surface waves are presented. In section 4, the contributions of surface waves to water level and mixing are evaluated and the relevant dynamics are discussed. In section 5, the conclusions are summarized.

2. Coupled Wave-Current Model and Numerical Experiments

2.1. NECOFS

[7] This study uses the coupled wave-current version of FVCOM within the NECOFS framework. NECOFS includes three model components: (1) a mesoscale meteorological model (MM5/WRF) [*Chen et al*., 2005]; (2) FVCOM [*Chen et al*., 2003, 2011a, 2011b]; and (3) SWAVE [*Qi et al*., 2009]. FVCOM was coupled with SWAVE through the traditional radiation stress approach [*Wu et al*., 2010]. MM5 is the fifth-generation NCAR/Penn State nonhydrostatic mesoscale model [*Dudhia and Bresch*, 2002], and WRF is the newer Weather Research and Forecast model [*Skamarock and Klemp*, 2008]. In NECOFS, MM5 was replaced by WRF after 2006 so that the background meteorological data used in this study are from MM5. The FVCOM system is described in detail in the FVCOM (version 3.1.6) manual [*Chen et al*., 2011a, 2011b]. Here, brief descriptions of FVCOM and SWAVE as used in this study are given.

2.2. FVCOM

[8] FVCOM is the unstructured grid finite-volume community ocean model, which was originally developed by *Chen et al*. [2003] and improved by the joint UMASSD and WHOI FVCOM development team [*Chen et al*., 2006, 2011a, 2011b]. The governing equations are discretized in an integral form over control volumes in which the advection terms are solved by a second-order accuracy upwind finite-volume flux scheme [*Kobayashi et al*., 1999; *Hubbard*, 1999] and time integration made using the modified explicit fourth-order Runge-Kutta (RK4) time-stepping scheme. FVCOM is implemented with two solvers: (1) a mode-split solver in which external and internal modes are advanced in tandem at different time steps, and (2) a semi-implicit solver with a single time step inversely proportional to water current magnitude. FVCOM is closed physically with the turbulent closure submodels: in the vertical is the Mellor and Yamada level 2.5 turbulence model as a default setup [*Mellor and Yamada*, 1982] with options in the General Turbulence Model [*Burchard*, 2002] and in the horizontal is the Smagorinsky turbulent parameterization [*Smagorinsky*, 1963]. The experiments described in this paper were conducted using the default setup and mode-split solver.

2.3. SWAVE

[9] SWAVE is an unstructured grid finite-volume version of the Simulating Wave Nearshore (SWAN) model [*Qi et al*., 2009]. SWAN was originally developed by *Booij et al*. [1999] and improved by the *SWAN Team* [2006a, 2006b]. SWAN features the wave action density spectrum balance equation. SWAVE was developed by implementing a flux-corrected transport algorithm in frequency space, an implicit Crank-Nicolson solver in directional space, and FVCOM finite-volume solvers in geographic space. This model was validated for both standard benchmark test problems and real wave simulation in the NECOFS domain [*Qi et al*., 2009].

2.4. FVCOM-SWAVE Setup

[10] Coupling of FVCOM and SWAVE is approached through the radiation stress, bottom boundary layer (BBL), and surface stress [*Wu et al*., 2010]. The radiation stresses are added into the FVCOM momentum equations to include the wave-driven motions. The BBL code with inclusion of the wave-current interaction developed by *Warner et al*. [2008] was converted into an unstructured grid finite-volume version using the FVCOM framework and then implemented into FVCOM. At the sea surface, the surface roughness used to calculate the wind stress is calculated using formulae described in *Donelan* [1993]. The coupling methods and equations are described in detail in R. C. Beardsley et al. (Coastal flooding in Scituate (MA): A FVCOM study of the Dec. 27, 2010 nor'easter, submitted to *Journal of Geophysical Research*, 2013).

[11] In this study, the coupled FVCOM and SWAVE models were configured for the computational domain, as shown in Figure 2, with a horizontal resolution varying from $\sim$300 m in the coastal region to 15 km in the open ocean. A hybrid terrain-following coordinate is used in the vertical with a total of 45 layers. In water depths $>$225 m, 10 uniform layers with a thickness of 5 m were specified in the upper 50 m and three uniform layers with the same thickness in the 15 m water column above the bottom, whereas in regions with water depth $\leq$225 m, a sigma coordinate was used with uniform layer thickness. The two vertical layer thickness schemes match at water depths of 225 m. This hybrid coordinate is designed to ensure the accurate simulation of the surface mixed layer and BBL on the

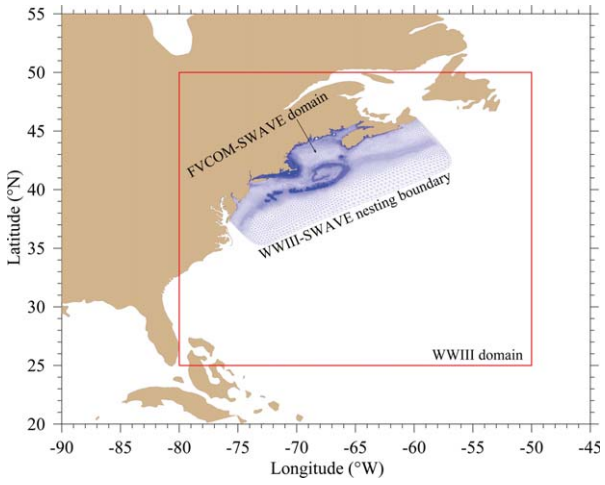

Figure 2. The computational domains for Wave Watch III (WWIII) and FVCOM/SWAVE. Red line indicates the boundary of the computational domain used for WWIII. The region consisting of unstructured triangular meshes is the NECOFS computational domain used for the fully wave-current-coupled FVCOM.

slope and other areas with strong bottom slopes. The wave parameters used in this study are shown in Table 1.

[12] The coupled model was run for the real-time simulation with inclusion of tidal, surface air pressure, surface wind stress, heat and moisture fluxes, and river discharge for the period 16–29 August 1991, during which time Hurricane Bob swept through this region on 19–20 August 1991. Running the model for stratified conditions allows us to examine the 3-D ocean responses to Hurricane Bob, not only for sea level evolution but also for turbulent mixing.

2.5. Surface Wind and Air Pressure Forcing

[13] The hurricane model used here is based on a symmetric wind field that becomes asymmetric by the motion of the hurricane center, using as input time series of central eye air pressure and location and maximum wind speed taken from the NWS 6-h records. The speed of the symmetric wind vector was calculated using the modified Rankin vortex model [*Phadke et al*., 2003] given as

$$|\mathbf{V}_{\mathrm{sym}}| = \begin{cases} V_{\max}\left(\dfrac{r}{R_{\max}}\right)^{X} & (r < R_{\max}) \\ V_{\max}\left(\dfrac{R_{\max}}{r}\right)^{X} & (R_{\max} \le r \le 3R_{\max}), \end{cases} \tag{1}$$

where $V_{\max}$ is the maximum wind speed; $R_{\max}$ is the radius of maximum winds; r is the radial distance from the hurricane center; and $X = 0.5$. $R_{\max}$ was estimated following *Vickery et al*. [2000] as

$$\ln R_{\max} = 2.173 - 0.0056748\Delta p + 0.0416289\psi, \tag{2}$$

where Δp is the pressure deficit defined as $\Delta p = P_n - P_c$; P_n is the surrounding atmospheric pressure; P_c is the hurricane central atmospheric pressure; and ψ is the latitude. Using data reported by *Pasch and Avila* [1992], *Houston et al*. [1999] derived that $\Delta p = 46$ mb and $P_c = 965$ mb near landfall in Rhode Island for Hurricane Bob. We used this value on an assumption that $P_n = 1011$ mb remained constant in time during the hurricane passage.

[14] The vortex wind vector was reduced in the planetary boundary layer to the vector wind at 10 m $\mathbf{V}_{10\mathrm{sym}} = 0.8 \cdot \mathbf{V}_{\mathrm{sym}}$ following *Powell and Black* [1990], and rotated inward relative to the isobars toward the vortex center by α was defined as

$$\alpha \begin{cases} 10^{\circ}\left(1 + \dfrac{r}{R_{\max}}\right) & 0 \le r \le R_{\max} \\ 20^{\circ} + 25^{\circ}\left(1 + \dfrac{r}{R_{\max}} - 1\right) & R_{\max} \le r \le 1.2R_{\max} \\ 25^{\circ} & r \ge 1.2R_{\max} \end{cases}. \tag{3}$$

following *Bretschneider* [1972]. The hurricane surface wind field was next calculated using the "correction" formula derived by *Jelesnianski* [1966] in which the motion of the hurricane was added to the adjusted 10-m symmetric wind vector as

$$\mathbf{V} = \mathbf{V}_{10\mathrm{sym}} + \left(\frac{r/R_{\max}}{1 + (r/R_{\max})^2}\right) \cdot \vec{V}_{\mathrm{path}} \tag{4}$$

where $\mathbf{V}$ is the total 10-m wind vector and $\mathbf{V}_{\mathrm{path}}$ is the velocity vector of the hurricane center along the hurricane path.

[15] The atmospheric pressure (P) was defined as the sum of the surrounding dynamics pressure (P_d) and the hurricane central atmospheric pressure (P_c), namely

$$P = P_c + P_d \tag{5}$$

with P_d determined by

$$\frac{\partial P_d}{\partial r} = \rho_{\mathrm{air}}\left(\frac{|\mathbf{V}_{\mathrm{sym}}^2|}{r} + f|\mathbf{V}_{\mathrm{sym}}^2|\right) \tag{6}$$

where f is the Coriolis parameter and the air density $\rho_{\mathrm{air}} = 1.18\mathrm{kg/m}^3$ (the density at 25°C and standard pressure (1013 mb).

[16] The hurricane model field was taken into account starting at 00:00 GMT on 16 August 1991. The two types of wind and air pressure fields were merged in the radial distance relative to the hurricane center. Inside the radial region of $r \le 1.5$ $R_{\max}$, the MM5 wind and air pressure were completely replaced by our hurricane model-predicted wind and air pressure. The radial distance between 1.5

Table 1. SWAVE Parameters

Parameters	Value
Frequency range (Hz)	0.05–0.5
Frequency bins	24
Direction	Full circle
Direction bins	36
Bottom friction	Jonswap formulation
Friction parameter	0.067
Minimum water depth (m)	0.05

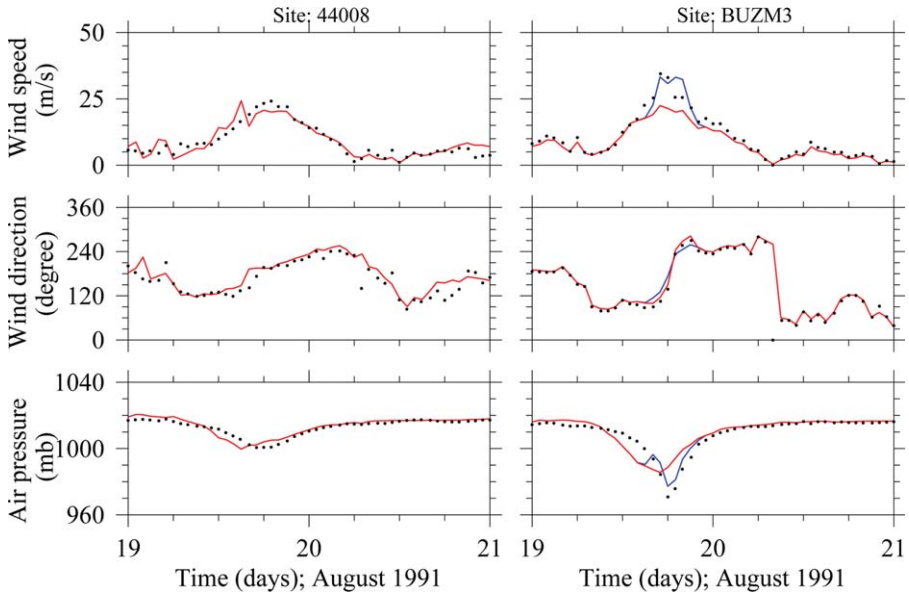

Figure 3. Comparisons between model-calculated and observed wind speed, wind direction, and air pressure at Buoy 44008 and BUZM3 during 19–21 August 1991: observed (black dots); MM5 calculated (red line); and calculated using the MM5 hurricane model combined fields (blue line).

R_{max} and 3 R_{max} defined the transition zone, in which the wind and air pressure fields were determined by a linear weight averaging of MM5 and hurricane model fields. The weight for the hurricane field (MM5) was 1 (zero) at 1.5 R_{max} and linearly decreased (increased) to zero (1) at 3 R_{max}. Outside of 3 R_{max}, only the MM5 fields were used. This method was validated by comparing the model-predicted wind and air pressures at coastal buoys (see the next section).

[17] The surface wind stress was calculated using $\tau = \rho_{air} C_d V^2$, where V is the combined 10-m wind speed and the drag coefficient C_d is specified by

$$C_d = \begin{cases} 1.0 \times 10^{-3} & 0 < V \le 4.0\text{m/s} \\ \left(1 + 1.5\dfrac{V - 4.0}{27 - 4.0}\right) \times 10^{-3} & 4.0\text{m/s} < V \le 27.0\text{m/s} \\ 2.5 \times 10^{-3} & V > 27.0\text{m/s} \end{cases}. \quad (7)$$

[18] This simplified formula was based on the 10-m neutral C_d computed using COARE3 [*Fairall et al*., 2003], COARE4 [*Edson*, 2009], and *Large and Pond* [1981] for wind speeds ≤26 m/s and more recent work showing that C_d reaches a maximum value in a range of 30–35 m/s and reduces at higher speeds [e.g., *Powell*, 2003; *Jarosz et al*., 2007; *Haus*, 2010]. Here, we cap C_d at a constant maximum value of 2.5×10^{-3} for wind speeds ≥27 m/s based on Figure 3 in *Jarosz et al*. [2007].

2.6. Open Boundary Forcing

[19] The open boundary conditions for FVCOM were specified using the Global-FVCOM hindcast assimilated fields through one-way nesting. Global-FVCOM was driven by (a) astronomical tidal forcing with eight constituents (M_2, S_2, N_2, K_2, K_1, P_1, O_1, and Q_1), (b) surface wind stress, (c) net heat flux at the surface plus shortwave irradiance in the water column, (d) surface air pressure gradients, (e) precipitation minus evaporation, and (f) river discharge. This model has been validated with a 50-year spin-up simulation and also used for a 33-year NECOFS hindcast simulation from 1978 to 2010. SWAVE's open boundary conditions were specified by nesting with Wave Watch III (WWIII). WWIII was configured for the northwestern North Atlantic basin (Figure 2) and run for the same period as FVCOM/SWAVE. The wave spectrum forcing was interpolated from WWIII to the open boundary nodes of SWAVE.

[20] To evaluate the importance of the wave-current interaction on the surge simulation, we made experiments for four cases: (I) only waves, (II) 3-D model run under stratified conditions without inclusion of waves, (III) 3-D model run under stratified conditions with inclusion of wave-current interaction, and (IV) the same as case III but under homogeneous conditions (with temperature and salinity treated as constant).

3. Simulation Results

3.1. Meteorological Forcing

[21] Wind and pressure data were recorded at 10 buoy stations during 16–29 August 1991 (Figure 1). Without coupling with the hurricane model, the MM5 hindcast significantly underestimated the observed maximum wind speed and minimum air pressure. With the combined MM5 hurricane model, the overall mean differences at stations computed for the period 19–21 August 1991 were 1.14 m/s for wind speed, 15.41° for wind direction, and 1.49 mb for air pressure, respectively (Tables 2 and 3 in which the wind direction circular statistics were computed using *Berens*' [2009] MATLAB CircStat toolbox). For example, at site BUZM3 at the entrance to Buzzards Bay located a radial

Table 2. Names of Observation Sites and the Ratio of the Closest Distance From a Site to the Storm Center Divided by R_{max}

Site ID	Site Name	Ratio
44005	Gulf of Maine 78 NM East of Portsmouth, NH	2.84
44007	Portland 12 NM Southeast of Portland, ME	0.09
44008	Nantucket 54 NM Southeast of Nantucket	3.90
44013	Boston 16 NM East of Boston, MA	1.47
44025	Long Island 33 NM South of Islip, NY	0.88
ALSN6	Ambrose Light, NY	0.19
BUZM3	Buzzards Bay, MA	0.49
IOSN3	Isle of Shoals, NH	0.83
MDRM1	Mt. Desert Rock, ME	1.20
MISM1	Matinicus Rock, ME	1.90
8410140	Eastport, ME	1.00
8411250	Cutler Naval Base, ME	1.01
8413320	Bar Harbor, ME	0.58
8418150	Portland, ME	0.50
8443970	Boston, MA	0.37
8447930	Woods Hole, MA	0.71
8449130	Nantucket Island, MA	1.54
8454000	Providence, RI	0.33
8452660	Newport, RI	0.00
8455083	Point Judith/Harbor of Refuge, RI	0.08
8461490	New London, CT	0.78
8510560	Montauk, NY	0.39
8518750	The Battery, NY	2.78
8536110	Cape May, NJ	2.93
8557380	Lewes, DE	3.03

distance of 0.49 R_{max} from the storm center at closest approach (Figure 1), the measured maximum wind speed at 10 m was 34.5 m/s and minimum pressure was 970.80 mb, whereas the MM5-computed maximum wind speed was only 22.5 m/s and minimum pressure was 985.63 mb (Figure 3). These large wind speed and pressure differences were reduced to 1.2 m/s for the maximum wind speed and to 7.1 mb for the minimum air pressure using the combined MM5 hurricane model fields. The combined MM5 hurricane model-derived wind speed and air pressure matched well with those derived only by MM5 before and after the hurricane passed. At National Data Buoy Center buoy 44008, located at a radial distance of 3.9 R_{max} from the storm center at closest approach, the MM5-derived wind speed and air pressure reasonably matched the buoy measurements, supportive of setting the hurricane model domain to a circle with radius 3 R_{max}. According to model-data comparisons at all available stations, the combined MM5 hurricane model was capable of reproducing the hurricane-derived surface wind and air pressure fields that were used to drive the coupled wave-current FVCOM for the Hurricane Bob-induced storm surge simulations. A relatively large standard deviation (SD) errors found in the wind direction was due to a significant variability of the wind direction of Hurricane Bob, and a small difference of the model-predicted wind direction from observations could lead to a big SD error.

3.2. Surface Waves

[22] The SWAVE-predicted surface waves exhibited a core of maximum significant wave height (H_s) on the right side of the hurricane center (Figure 4). H_s increased as Hurricane Bob moved northeastward along the shelf break and decreased after Hurricane Bob entered the shelf and made landfall. For example, the maximum H_s reached 14.0 m at 06:00 GMT on 19 August 1991, grew to 21.4 m at 12:00 GMT on 19 August 1991, and then dropped to 17.0 m at 18:00 GMT on 19 August 1991. It is clear that the primary influence of hurricane-driven waves was limited to the right side of the hurricane track on the regional scale.

[23] Surface wave measurements were made at six buoys over the continental shelf and at near-coastal sites during Hurricane Bob (16–29 August 1991; Figure 1). With the combined MM5 hurricane wind field, the model-predicted significant wave heights (H_s) and peak frequencies (T_p) were in reasonable agreement with the observations. For case I in which SWAVE was run without coupling to ocean currents, the overall SD errors at six buoy sites (estimated based on the time series over 16–29 August 1991) for H_s and T_p were 0.20 m and 0.71 s, respectively (Table 4). Including wave-current interaction in case III caused very small changes in the statistics (Table 4). Figure 5 shows time series comparisons at two New England shelf buoys: 44008 (south of Nantucket Shoals at 3.9 R_{max} on the right side of the hurricane track) and 44025 (south of Long Island at 0.9 R_{max} on the left side of the hurricane track). The observed maximum H_s was 5.6 m higher at buoy 44008 than at buoy 44025. Although SWAVE

Table 3. Errors of Model-Computed 10 m Wind Velocity East and North Components and Surface Air Pressure Over the Period of 19–21 August 1991 at Buoy and Coastal Stations

	Wind Speed (m/s)		Wind Direction (degree)		P (mb)	
Station ID	Difference	Standard	Difference	Standard	Difference	Standard
44005	1.82	3.66	10.36	23.96	2.59	1.53
44007	0.50	1.89	2.27	13.41	0.76	1.49
44008	0.18	2.32	7.84	18.86	0.68	1.05
44013	1.37	3.58	20.37	35.09	1.22	2.34
44025	1.15	2.38	2.19	20.85	1.42	1.03
ALSN6	0.09	4.77	−15.41	44.74	0.69	2.57
BUZM3	−0.53	1.77	2.41	13.80	0.97	1.66
IOSN3	0.42	3.98	15.02	53.08	0.83	2.05
MDRM1	−0.77	1.51	2.37	14.57	0.54	1.48
MISM1	−1.45	4.04	11.80	48.88	1.16	1.98
Average	0.28	2.99	5.92	28.72	2.59	1.53
Standard Deviation	1.01	1.14	9.76	15.41	0.76	1.49

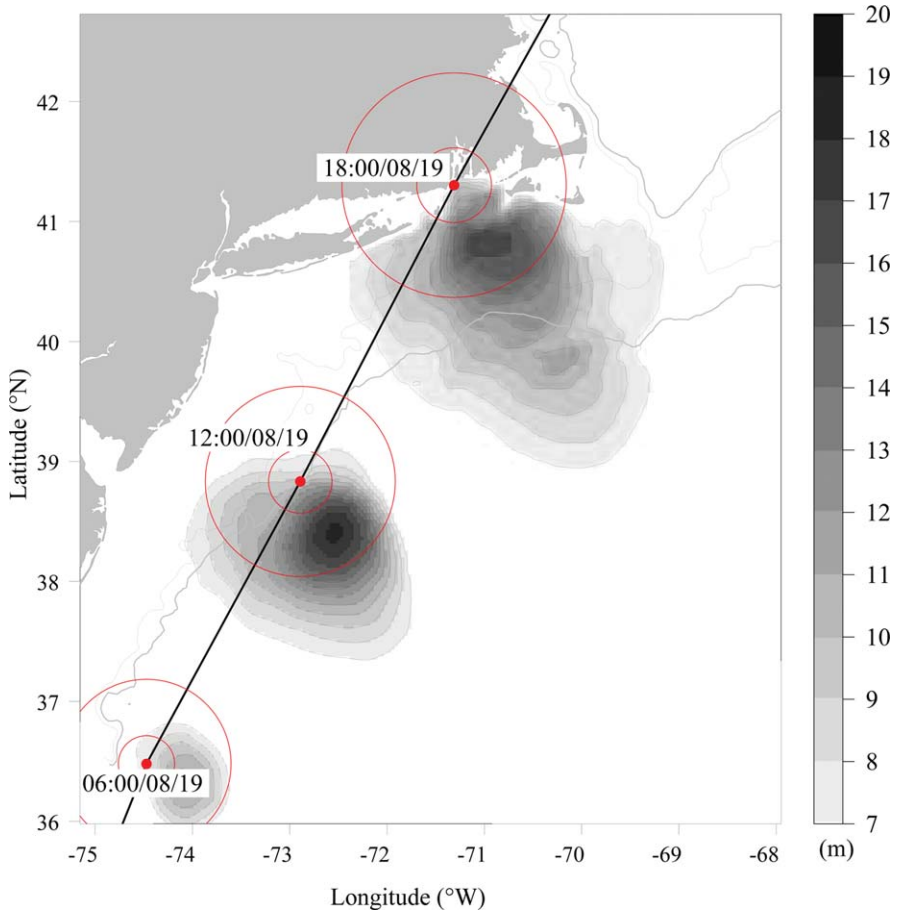

Figure 4. Spatial distributions of model-predicted significant wave heights along the hurricane track at 06:00, 12:00, and 18:00 GMT on 19 August 1991. The red circles centered at each site are drawn with radii equal to 1 R_{max} and 3 R_{max}.

underestimated the maximum H_s at 44008 by less than 1 m and overestimated H_s at 44025 by ~2 m, the asymmetry characteristics in the wave field were well captured by SWAVE. The comparison results for cases I and III suggest that (1) wave-current interaction produced a slightly higher wave peak at buoy 44008, although the overall simulation accuracy was slightly improved, and (2) as long as the significant wave height and peak period are considered, the feedback influence of wave-current interaction to surface wave simulation was insignificant (based on Table 4).

3.3. Water Elevation

[24] Model-predicted water elevation was compared directly to observed elevation at the 15 coastal tidal gauges available in the model domain (Figure 6 and Tables 5 and 6). To better view the contribution of wave-current

Table 4. Errors of Model-Computed Significant Wave Heights and Peak Periods for the Cases Without and With Wave-Current Interaction Over the Period of 16–29 August 1991 at Available Measurement Stations

	Case I				Case III			
	H_s (m)		T_p (s)		H_s (m)		T_p (s)	
Site ID	Difference	Standard	Difference	Standard	Difference	Standard	Difference	Standard
44005	−0.02	0.29	0.10	0.58	−0.02	0.29	0.10	0.61
44007	−0.26	0.38	1.23	2.00	−0.26	0.35	1.30	1.99
44008	0.19	0.47	1.44	1.98	0.17	0.47	1.55	2.03
44013	−0.72	0.87	1.60	2.80	−0.72	0.84	1.65	2.80
44025	0.16	0.53	1.48	1.89	0.16	0.52	1.44	1.99
ALSN6	−0.01	0.60	1.46	1.81	−0.02	0.60	1.47	1.94
MEAN	−0.11	0.53	1.22	1.84	−0.11	0.51	1.25	1.89
Standard Deviation	0.34	0.20	0.56	0.71	0.34	0.20	0.58	0.71

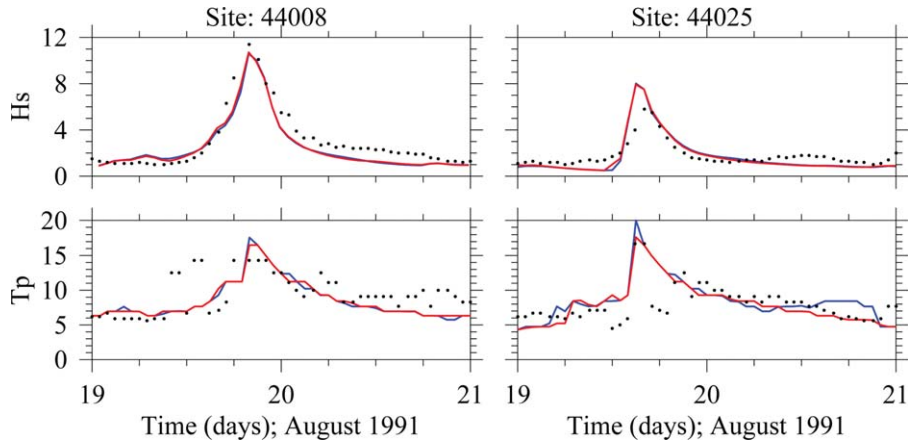

Figure 5. Comparisons between model-computed and observed significant wave heights and peak periods during 19–21 August 1991 at Buoys 44008 and 44025: observed (black dots); calculated without inclusion of wave-current interaction (red line); and calculated with inclusion of wave-current interaction (blue line).

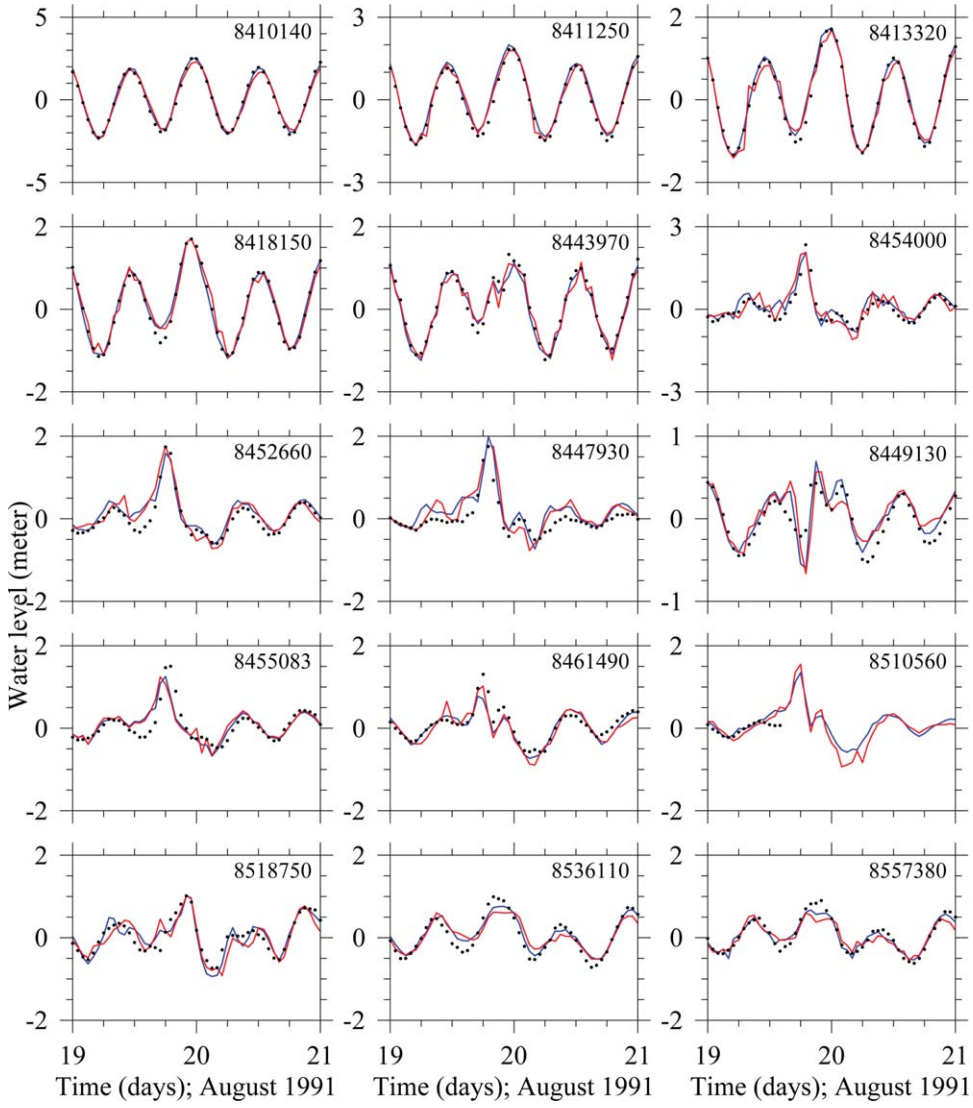

Figure 6. Comparison between model-computed and observed water elevations during 19–21 August 1991 at 15 tidal gauges along the coast: observed (black dots); calculated without inclusion of wave-current interaction (blue line); and calculated with inclusion of wave-current interaction (red line).

Table 5. Observed Maximum Water Level Elevation, Tidal Elevation, and Surge at the Time of Maximum Water Level Elevation at the 15 Available Tidal Stations[a]

Site ID	Site Name	Highest Water Level (m)	Tidal Elevation (m)	Surge (m)	Date and Time (GMT)
8410140	Eastport, ME	2.47	2.26	0.21	19 August 1991; 23:00
8411250	Cutler Naval Base, ME	1.83	1.5	0.34	20 August 1991; 00:00
8413320	Bar Harbor, ME	1.7	1.31	0.39	20 August 1991; 00:00
8418150	Portland, ME	1.7	1.15	0.54	19 August 1991; 23:00
8443970	Boston, MA	1.3	1.17	0.13	19 August 1991; 23:00
8447930	Woods Hole, MA	1.77	0.14	1.63	19 August 1991; 19:00
8449130	Nantucket Island, MA	0.41	0.02	0.39	19 August 1991; 21:00
8454000	Providence, RI	2.39	0.43	1.96	19 August 1991; 19:00
8452660	Newport, RI	1.78	0.22	1.56	19 August 1991; 18:00
8455083	Point Judith, RI	1.5	0.38	1.12	19 August 1991; 19:00
8461490	New London, CT	1.29	−0.06	1.34	19 August 1991; 18:00
8510560	Montauk, NY	0.65	0.58	0.07	19 August 1991; 01:00
8518750	The Battery, NY	0.99	0.54	0.44	19 August 1991; 22:00
8536110	Cape May, NJ	1	0.65	0.35	19 August 1991; 20:00
8557380	Lewes, DE	0.89	0.61	0.28	19 August 1991; 22:00
Standard Deviation		0.59	0.63	0.62	

[a]Site 8510560 data are missing from 19 August 1991 (14:00) to 18 October 1991 (23:00).

interaction to the sea level change along the coast, we plotted the observed and model-predicted maximum water elevations at the stations from north to south in Figure 7 and grouped these stations into five zones: zone 1 (northern GoM: Eastport, ME; Cutler Naval Base, ME; and Bar Harbor, ME); zone 2 (western GoM: Portland, ME and Boston, MA); zone 3 (transition zone: Woods Hole, MA and Nantucket Island, MA); zone 4 (all stations near where the hurricane made landfall: Providence, RI; Newport, RI; Point Judith, RI; New London, CT; and Montauk, NY); and zone 5 (further south: The Battery, NY; Cape May, NJ; and Lewes, DE). The surges were largest in zones 3–4, whereas larger differences of the model-predicted surge level between cases II and III without and with wave–current interactions mainly occurred in zone 4. The Montauk station stopped reporting at 14:00 GMT on 19 August 1991 so no surge was seen there. Including wave-current interaction improved the simulation of maximum surge level at the New

Table 6. Difference Between Model-Computed and Observed Maximum Water Elevations at the 15 Tidal Stations for the Cases Without (Case II) and With (Case III) Wave-Current Interaction

		Maximum Difference	
Site ID	Site Name	Case II	Case III
8410140	Eastport, ME	0.03	−0.09
8411250	Culter Naval Base, ME	0.10	−0.10
8413320	Bar Harbor, ME	0.03	−0.02
8418150	Portland, ME	0.00	0.01
8443970	Boston, MA	−0.09	−0.13
8447930	Woods Hole, MA	0.17	0.30
8449130	Nantucket Island, MA	0.23	0.25
8454000	Providence, RI	−0.32	−0.33
8452660	Newport, RI	−0.21	−0.03
8455083	Point Judith, RI	−0.25	0.01
8461490	New London, CT	−0.52	−0.27
8510560	Montauk, NY	0.00	0.20
8518750	The Battery, NY	0.01	0.01
8536110	Cape May, NJ	−0.26	−0.41
8557380	Lewes, DE	−0.24	−0.31
Standard Deviation		0.20	0.21

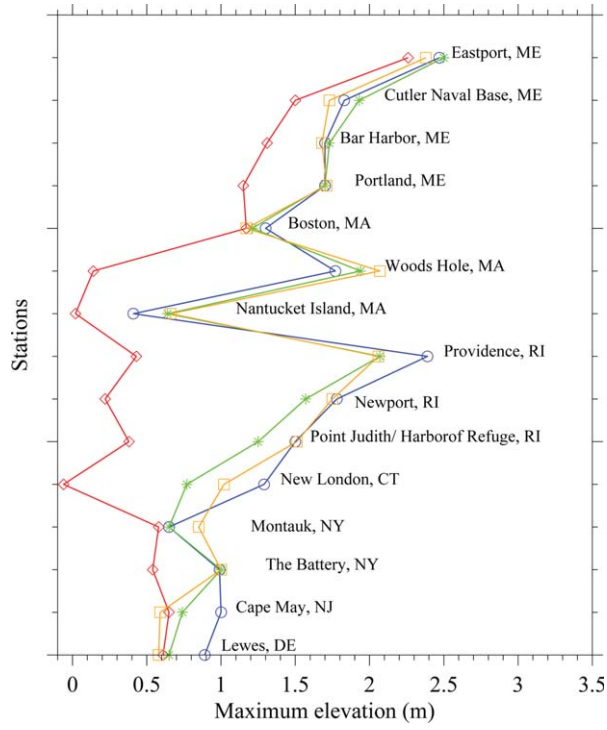

Figure 7. Distribution of the model-predicted and observed maximum water elevations at available coastal stations from Eastport (ME) to Lewes (DE) during 19–21 August 1991. To identify the surge elevation component, we also include the tidal elevation at the time when the maximum water elevation was observed in this figure: observed (blue line); computed for case II with no wave–current interaction (green line); computed for case III with wave-current interaction (orange line); and tidal elevation (red line).

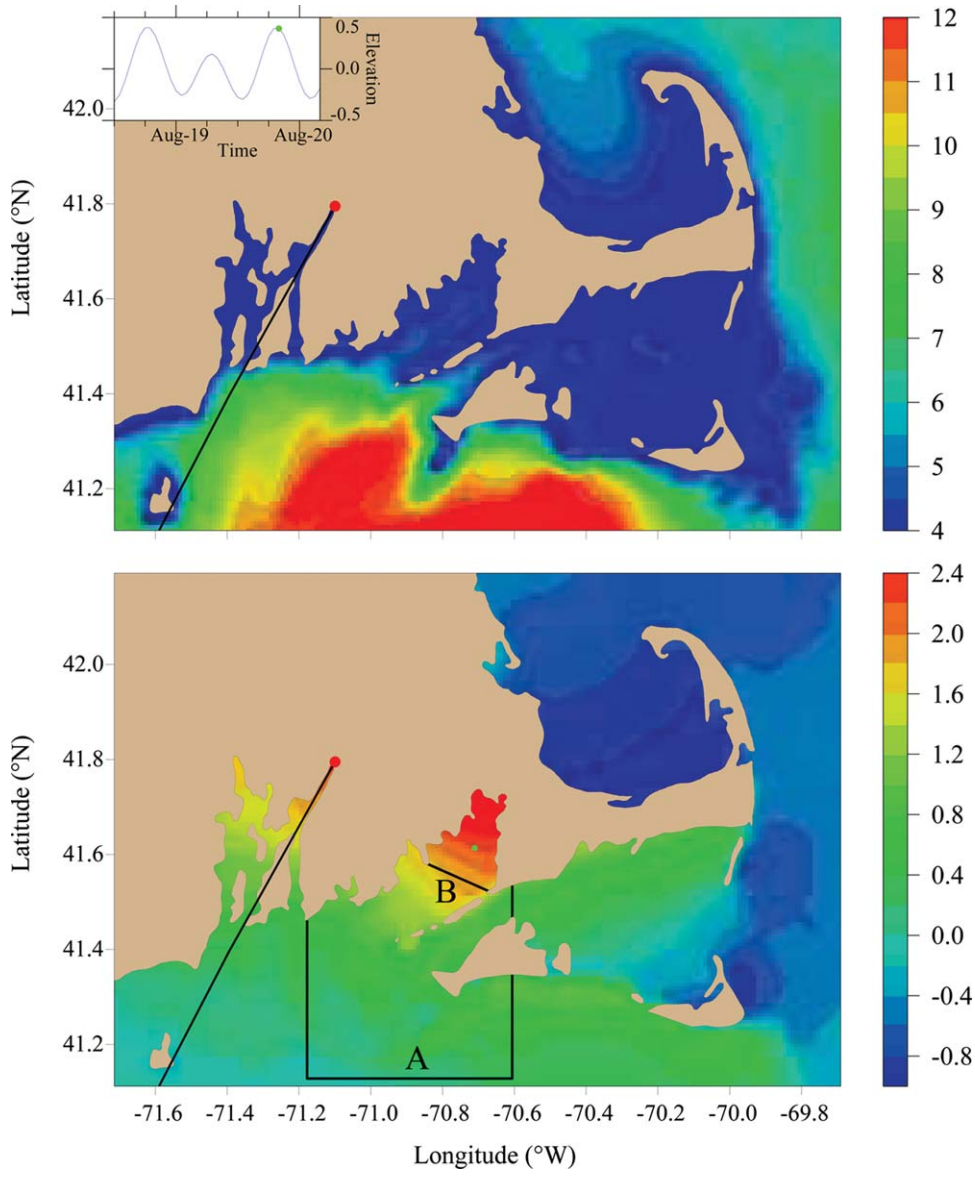

Figure 8. Snapshots of the spatial distribution of model-computed significant wave height (upper) and water elevation (lower) in meters at 19:00 GMT on 19 August 1991 over the New England shelf and coastal waters. At this moment, the highest water elevation in Buzzard Bay occurred. The black line with a red dot at the end shows the hurricane track and location of the hurricane center at the time that the images were plotted. Black lines marked as "A" and "B" define sections A and B used to compare net water flux calculations.

London, Point Judith, and Newport stations by approximately 10–25 cm; however, no significant difference was found at Providence where the highest surge was observed. The surge was relatively low in zone 1, where the hurricane-induced sea level rise was approximately 10–40 cm. Although the difference of the model-predicted surge level between cases II and III was ~20 cm at Cutler Naval Base, it was small at Bar Harbor and Eastport. In zone 2, the largest surge appeared at Portland and was well captured by the model; however, no significant difference was found in the surge level between the cases without and with wave-current interaction.

[25] The model was capable of reproducing the observed peaks and oscillations before, when, and after the hurricane passed these coastal stations. The Woods Hole and Nantucket Island stations were located in Buzzard Bay and Nantucket Sound on the right side of the hurricane track. The observed maximum water elevations were 1.75 and 0.51 m at these two stations, respectively, which were captured reasonably well by the model. The observation reported the highest surge at Providence, RI, and significantly lower surge at Boston, MA. This spatial distribution was reproduced by the model.

[26] In summary, the contribution of wave-current interaction to the surge varied significantly in space and time. Although the overall SD errors for the surge elevation remained almost the same between the cases without and with wave-current interaction, it still accounts for

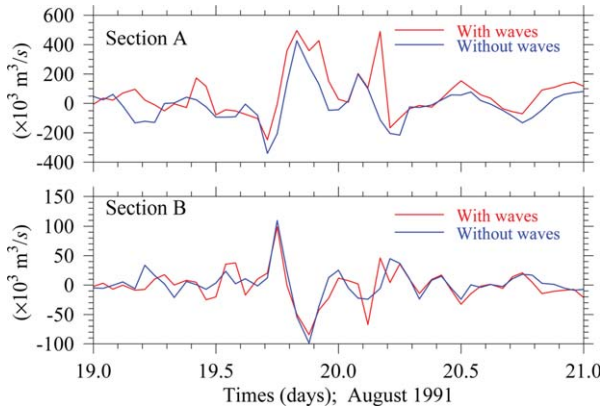

Figure 9. Net water fluxes through section A (upper) and section B (lower) during 19–21 August 1991 for the model runs with (red line) and without (blue line) wave-current interactions.

10%–17% of the water rise when the hurricane passed. This result is consistent with previous studies done by *Huang et al*. [2010], who used a one-way coupled FVCOM-SWAN model to simulate a hypothetical hurricane-induced storm surge in Tampa Bay, FL. This difference may be sufficient to raise sea level above the critical level for flooding.

4. Discussion

4.1. Contributions of Wave-Current Interaction to Water Elevation

[27] One of the key findings from our experiments is that the contribution of wave-current interaction to the Hurricane Bob-derived maximum water elevation varied significantly in space and time along the New England coast. It was significant along the southern coast from New London to Newport, but insignificant at Providence, Nantucket, Woods Hole, Boston, and further north along the coast. Particularly at Providence in Narragansett and Buzzard Bay, including wave-current interaction did not show an improvement in the surge simulation. One interpretation is related to the hurricane track. Hurricane Bob came ashore near the mouth of Narragansett Bay. The hurricane-induced maximum sea level in Buzzards Bay occurred around high tide at 19:00 GMT on 19 August 1991, at which time significant wave heights were high over the shelf (∼12 m or over) but not in the Bay (∼4 m) (Figure 8). This was also the time at which the highest significant wave height in the Bay was observed.

[28] According to the incompressible continuity equation, the change of water elevation in a region is equaled to the change of the net water transport through this region. In addition to the change of drag forces at the surface and bottom, wave-current interaction added an additional radiation stress to the momentum equations, which can directly change the speed and direction of the water movement and thus water transport. As the change of water elevation is controlled by a net flux rather than water velocity itself, the contribution of wave-current interaction to the water elevation could only be significant if this interaction leads to large local divergence and convergence of water transport. Creating a closed box with boundaries running across Vineyard Sound, Nantucket Shoal, and Buzzards Bay (Figure 8), we calculated the net water flux during the hurricane passage for cases II and III (without and with wave-current interaction). Figure 9 shows the comparisons for these two cases on sections A and B over the period 19–21 August 1991. Over the shelf, fluxes estimated from these two cases do show noticeable difference. With wave-current interaction, the net maximum flux was about 14% higher around 19:00 GMT on 19 August 1991, and a second peak was predicted in early 20 August 1991. This difference showed little influence on the net flux into Buzzard Bay through

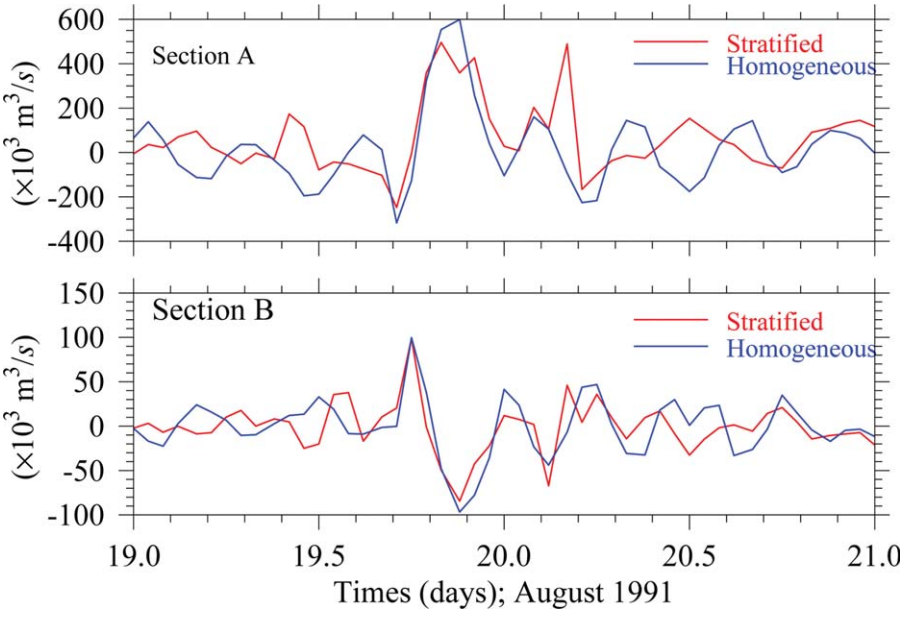

Figure 10. Net water fluxes through section A (upper) and section B (lower) during 19–21 August 1991 for the model runs with homogenous (blue line) and stratified (red line) ocean conditions.

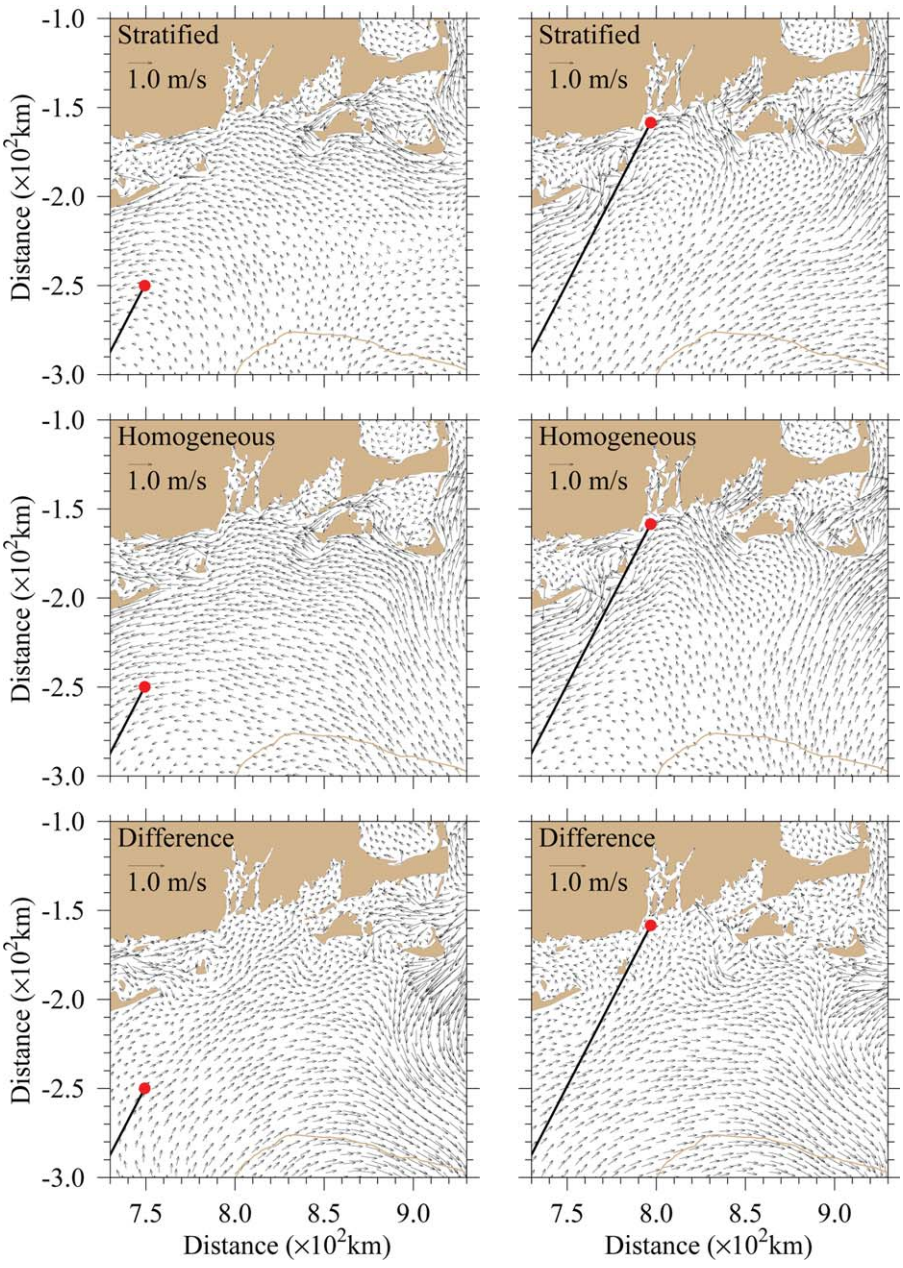

Figure 11. Distributions of model-computed vertically averaged currents and their differences (bottom) at 16:00 and 18:00 GMT on 19 August 1991 under stratified (top) and homogenous (middle) ocean conditions. The black lines with red dots at the end show the hurricane track and location at 16:00 and 18:00 GMT on 19 August 1991, respectively.

section B, where the maximum difference between cases II and III was 2.2%. This result suggests that during the passing of Hurricane Bob, the influence of wave-current interaction to surge elevation was more significant over the shelf than inside the Bay. This helps explain why a significant difference was found at coastal stations from New London to Newport but not at Providence and inside Buzzard Bay.

4.2. Role of Stratification

[29] Unlike most previous hurricane-induced storm surge simulations, our experiments were made for a 3-D case with inclusion of water temperature and salinity. *Weisberg and Zheng* [2008] compared 2-D and 3-D storm surge simulation results in Tampa Bay, FL, and recommended a 3-D approach to include more realistic dynamics governing storm surge. *Dukhovskoy and Morey* [2011] applied a 3-D FVCOM to simulate the Hurricane Dennis-induced storm surge and found a strong vertical shear in the water currents in homogenous conditions, which could contribute to the sea level change in coastal regions. *Orton et al*. [2012] estimated an impact of stratification on storm surge in the estuaries around New York City and reported that stratification accounted for approximately 6%–13% for the peak

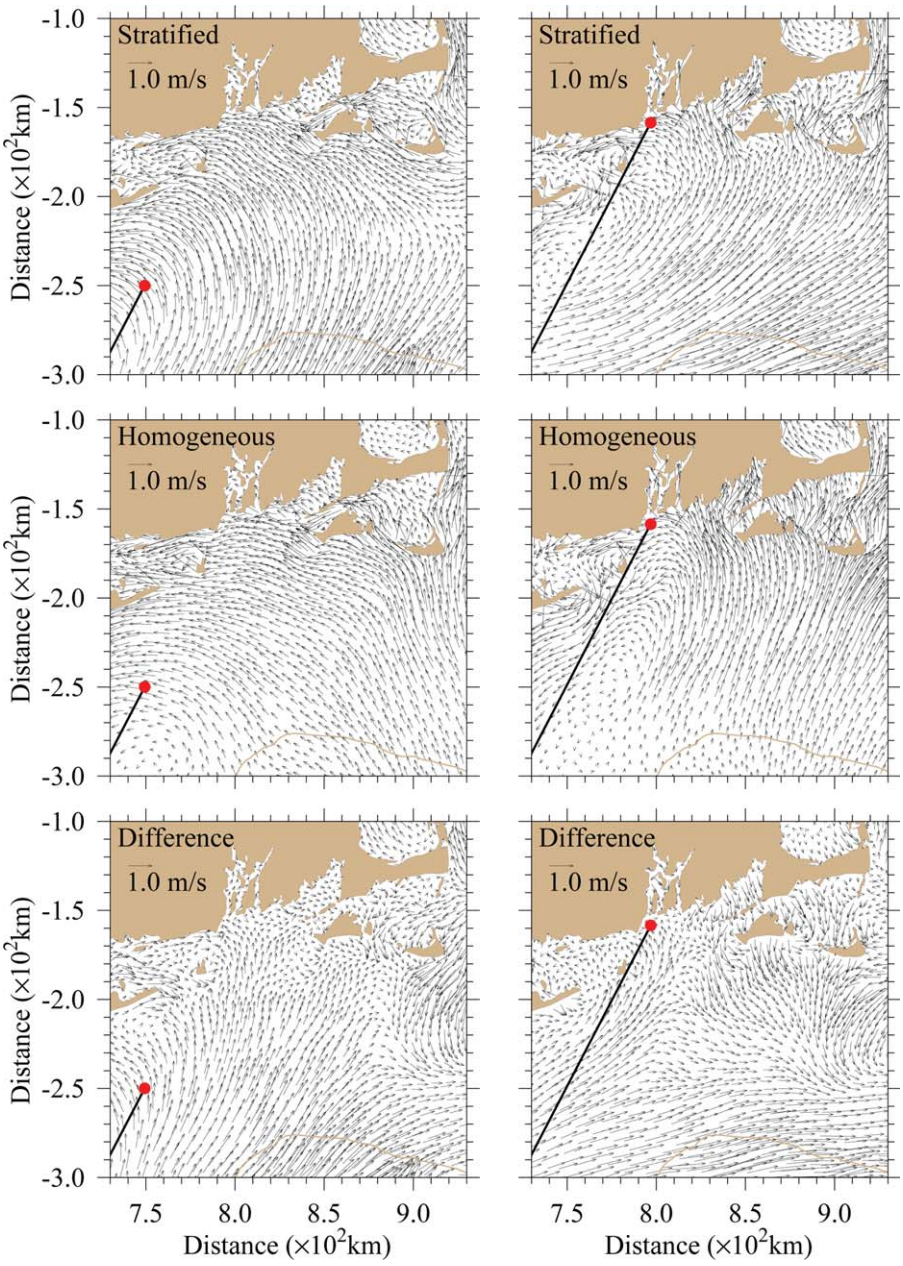

Figure 12. Distributions of model-computed near-surface currents and their differences (bottom) at 16:00 and 18:00 GMT on 19 August 1991 under stratified (top) and homogenous (middle) ocean conditions. As in Figure 11, the hurricane track and location are denoted by the black lines with red dots at the end.

water elevation in those estuaries. One question here is that should one include stratification for storm surge simulation over the New England shelf, particularly in a stratified coastal region? To address this question in our cases, we reran our model by removing water temperature and salinity (case IV) and compared the results with case III that included stratification.

[30] Time series of the net fluxes through section A show that the primary maximum flux peak predicted without stratification on late 19 August 1991 is ~11.5% higher than with stratification, whereas the secondary peak on early 20 August 1991 is underpredicted (Figure 10). The general shape of the net flux time series during that period without stratification is similar to case II with stratification but not wave-current interaction (Figure 9). Both before and after that period, the cases III and IV net flux time series differed qualitatively for reasons unknown.

[31] On section B, little difference (<2.9%) was found for the maximum flux between stratified and homogenous cases. This result is not surprising, because the water in Buzzard Bay was vertically well mixed during the Hurricane Bob event.

[32] The northeast U.S. continental shelf is characterized by numerous islands (e.g., Block Island, Nantucket Island, Martha's Vineyard, and Long Island), and the water around these islands is generally stratified during the summer

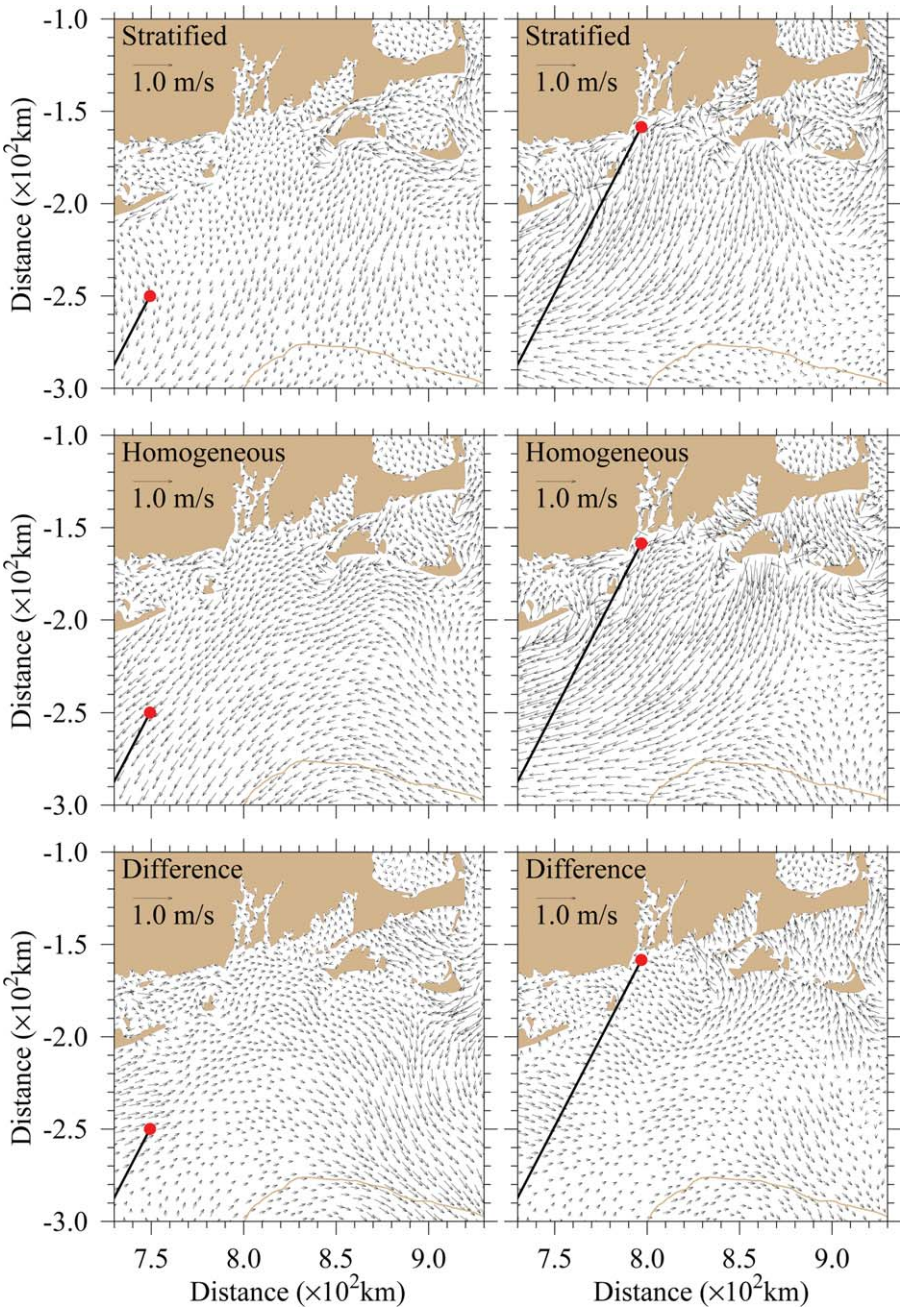

Figure 13. Distributions of model-computed near-bottom currents and their differences (bottom) at 16:00 and 18:00 GMT on 19 August 1991 under stratified (top) and homogenous (middle) ocean conditions. As in Figure 11, the hurricane track and location are denoted by the black lines with red dots at the end.

season. For example, Coastal Ocean Dynamics Application Radar measurements made during 2000–2008 detected relatively strong around-island currents (like a clockwise eddy around the tip of Long Island) [*Ullman and Codiga*, 2004]. The current pattern exists there throughout the year, but its intensity varies with winds and stratification. As a result of the existence of buoyancy-driven flow over the shelf, currents and water transport can differ significantly in the cases with and without inclusion of stratification. Figure 11 shows that the water transports in most shallow regions were relatively similar for homogenous and stratified cases, but did exhibit large differences over the shelf where the water was stratified. The homogenous case predicted much larger onshore transport over the shelf than the stratified case with noticeable differences in direction. East of Nantucket Sound is an area where a strong tidal mixing front is located, whether or not including stratification could strongly influence the current field in this region.

[33] The redistribution of bottom sediment due to hurricanes and nor'easter storms has received increased attention over the New England Shelf. The BBL dynamics

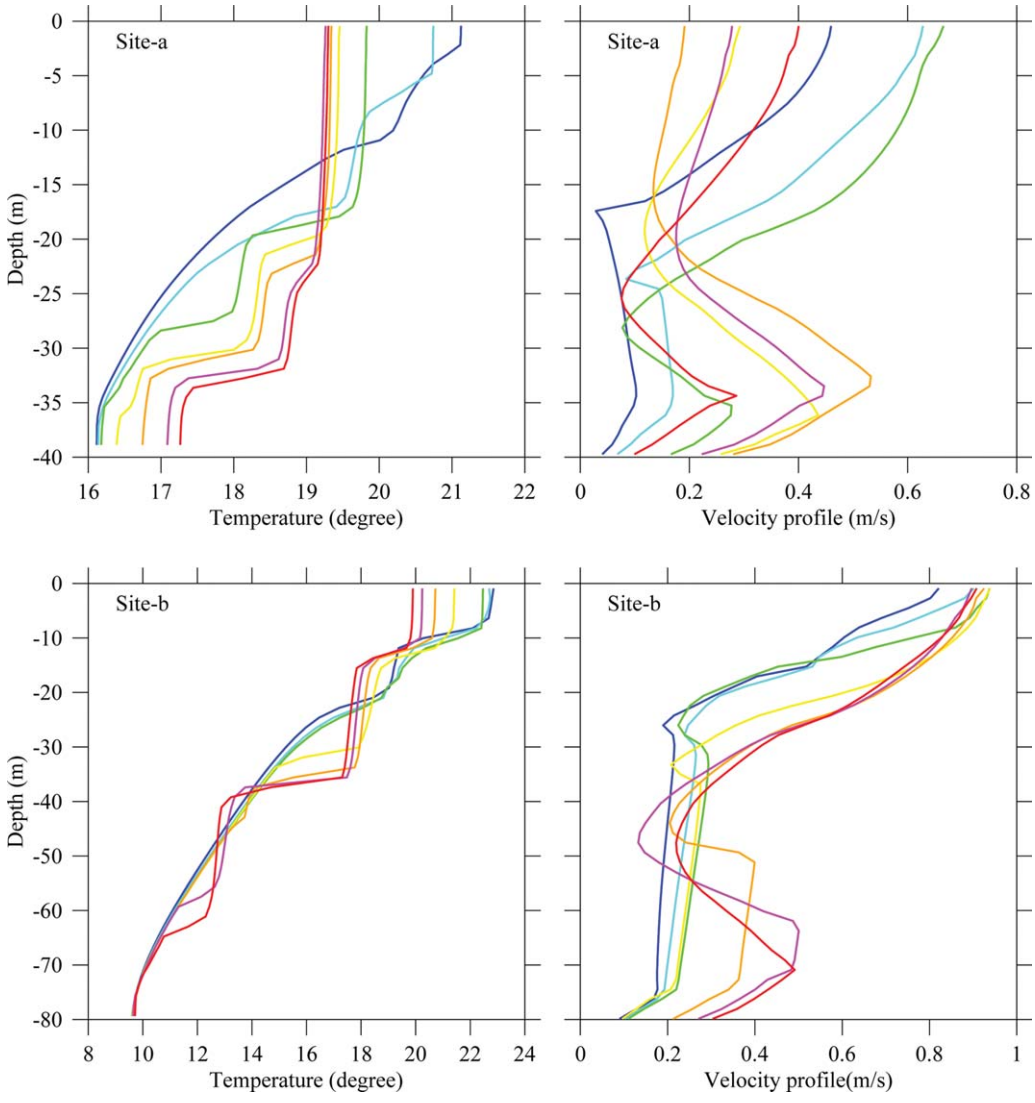

Figure 14. Vertical profiles of water temperature (left) and velocity (right) before and after Hurricane Bob passed by site a (top) and site b (bottom). Blue, cyan, and green lines were taken with an hourly time interval in 3 h before Hurricane Bob arrived at the sites. Magenta, orange, and yellow lines were taken with an hourly time interval in 3 h after Hurricane Bob passed the sites. The zero time is 18:00 GMT on 19 August 1991 at site a and 15:00 GMT on 19 August 1991 at site b.

associated with wave-current interaction are one of the key physical processes that drive morphological change of the seabed. This interaction could differ in cases with and without stratification. Figures 12 and 13 show comparisons of water currents at the sea surface and near the bottom at 16:00 GMT and 18:00 GMT on 19 August 1991 as Hurricane Bob crossed the shelf. The surface and near-bottom currents clearly differ without and with stratification. In the stratified case, the model predicted stronger surface currents in the stratified shelf region as a result of surface mix layer dynamics, with differences as large as ~100 cm/s, leading to different near-bottom currents near and around the islands. When the Hurricane Bob center moved close to Narragansett Bay, the homogenous case significantly under predicted the offshore near-bottom current over the shelf south of Long Island. In Nantucket Sound, the model-predicted near-bottom currents were opposite in direction in the homogenous and stratified cases. The direction of the near-bottom currents also differed in Buzzards Bay. These results suggest that if we want to simulate the hurricane-induced sediment transport near the bottom over the continental shelf where the water is generally stratified, we should consider including stratification.

[34] Vertical profiles of the water velocity and temperature varied with vertical mixing induced by Hurricane Bob (Figure 14). For example, at site a (located at 71.2°W, 41.2°N; see Figure 1), before Hurricane Bob passed, the surface mixed layer thickness was about 10 m, with surface-intensified currents. The surface mixed layer deepened as Hurricane Bob approached this site. At the time when the wind reached its maximum, the water was mixed down to a depth of approximately 30–35 m. As a result, the currents were intensified near the bottom. At site b on the shelf (located at 71.7°W, 40.3°N; see Figure 1), the water was

initially strongly stratified. The hurricane-induced strong winds mixed the upper 30-m of the water column, producing a strong vertical velocity shear in the lower water column, conditions that persisted during the hurricane passage.

5. Conclusions

[35] Using the 3-D fully wave-current coupled FVCOM system, we examined the impact of wave-current interaction on the coastal ocean during the passage of Hurricane Bob over the New England shelf. We conducted four process-oriented case studies to assess the influence of wave-current interaction in simulating surface waves and surge elevation under homogenous and stratified ocean conditions. The results show that the effect of wave-current interaction on storm surge varied in space and time: very important along the southern coast from New London to Newport but nearly insignificant at Providence, Nantucket, Woods Hole, Boston, and further north along the northern coast. Although the water was generally vertically well mixed near the coast, it was strongly stratified over the continental shelf and around islands in the coastal region. The hurricane-induced wave-current interaction generated strong vertical shear of water currents in the stratified area and thus produced a strong offshore transport near the bottom and enhanced water mixing over the continental shelf. The background circulation associate with stratification resulted in a significant difference of water currents around islands during the passage of Hurricane Bob. Our results suggest that stratification should be included in storm surge simulation in the northeast continental shelf region as many of the islands in the continental shelf region are surrounded by stratified waters during much of the year.

[36] **Acknowledgments.** This work was supported by the MIT Sea Grant College Program through grant 2012-R/RC-127 and the NOAA NERACOOS Program funds for NECOFS. The development of the FVCOM system has been supported by the NSF Ocean Sciences Division through grants OCE-0234545, OCE-0227679, OCE-0606928, and OCE-0712903 and the NSF Office of Polar Programs-Arctic Sciences Division through grants ARC0712903, ARC0732084, ARC0804029, and ARC1203393. C.C.'s contribution was also supported by Shanghai Ocean University International Cooperation Program (A-2302-11-0003), the Program of Science and Technology Commission of Shanghai Municipality (09320503700), and the Leading Academic Discipline Project of Shanghai Municipal Education Commission (J50702).

References

Berens, P. (2009), CirStat: A MATLAB Toolbox for Circular Statistics, *J. Stat. Soft.*, *31*, 1–21.

Booij, N., R. C. Ris, and L. H. Holthuijsen (1999), A third-generation wave model for coastal regions: 1. Model description and validation, *J. Geophys. Res.*, *104*(C4), 7649–7666, doi:10.1029/98JC02622.

Bretschneider, C. L. (1972), A non-dimensional stationary hurricane wave model, paper presented at 4th Offshore Technology Conference, Houston, Tex.

Burchard, H. (2002), Applied turbulence modeling in marine waters, *Lecture Notes in Earth Sciences 100*, vol. *215*, Springer, Berlin.

Chen, C. S., H. D. Liu, and R. C. Beardsley (2003), An unstructured grid, finite-volume, three-dimensional, primitive equations ocean model: Application to coastal ocean and estuaries, *J. Atmos. Oceanic Technol.*, *20*, 159–186, doi:10.1175/1520-0426(2003)020.

Chen, C., R. C. Beardsley, S. Hu, Q. Xu, and H. Lin (2005), Using MM5 to hindcast the ocean surface forcing fields over the Gulf of Maine and Georges Bank region, *J. Atmos. Oceanic Technol.*, *22*, 131–145, doi:10.1175/JTECH-1682.1.

Chen, C., R. C. Beardsley, and G. Cowles (2006), An unstructured grid, finite-volume coastal ocean model (FVCOM) system, *Oceanography*, *19*, 78–89, doi:10.5670/oceanog.2006.92.

Chen, C., J. Qi, C. Li, R. C. Beardsley, H. Lin, R. Walker, and K. Gates (2008), Complexity of the flooding/drying process in an estuarine tidal-creek salt-marsh system: An application of FVCOM, *J. Geophys. Res.*, *113*, C07052, doi:10.1029/2007jc004328.

Chen, C., H. Huang, R. C. Beardsley, Q. Xu, R. Limeburner, G. W. Gowles, Y. Sun, J. Qi, and H. Lin (2011a), Tidal dynamics in the Gulf of Maine and New England Shelf: An application of FVCOM, *J. Geophys. Res.*, *116*, C12010, doi:10.1029/2011JC007054.

Chen, C., et al. (2011b), An Unstructured Grid, Finite-Volume Community Ocean Model FVCOM User Manual, 3rd ed., *SMAST/UMASSD Tech. Rep. 11–1101*, p. 373, SMAST, Mass.

Cheung, K. F., L. Tang, J. P. Donnelly, E. M. Scileppi, K. B. Liu, X. Z. Mao, S. H. Houston, and R. J. Murnane (2007), Numerical modeling and field evidence of coastal overwash in southern New England from Hurricane Bob and implications for paleotempestology, *J. Geophys. Res.*, *112*, F03024, doi:10.1029/2006JF000612.

Donelan, A. M., F. W. Dobson, S. D. Smith, and R. J. Anderson (1993), On the dependence of sea surface roughness on wave development, *J. Phys. Oceanogr.*, *23*, 2143–2149, doi:10.1175/1520-0485(2001)031.

Dudhia, J., and J. F. Bresch (2002), A global version of the PSU-NCAR Mesoscale Model, *Mon. Weather Rev.*, *130*(12), 2989–3007, doi:10.1175/1520-0493(2002)130.

Dukhovskoy, D. S., and S. L. Morey (2011), Simulation of the Hurricane Dennis storm surge and considerations for vertical resolution, *Nat. Hazards*, *58*, 511–540, doi:10.1007/s11069-010-9684-5.

Edson, J. (2009), *Review of air-sea transfer processes, paper presented at ECMWF Workshop 2008 on Ocean-Atmosphere Interactions*, Reading, England.

Fairall, C. W., E. F. Bradley, J. E. Hare, A. A. Grachev, and J. B. Edson (2003), Bulk parameterization of air-sea fluxes: Updates and verification for the COARE algorithm, *J. Clim.*, *16*, 571–591, doi:10.1175/1520-0442(2003)016.

Haus, B. K., D. Jeong, M. A. Donelan, J. A. Zhang, and I. Savelyev (2010), Relative rates of sea-air heat transfer and frictional drag in very high winds, *Geophys. Res. Lett.*, *71*, GL042206, doi:10.1029/2009GL042206.

Houston, S. H., W. A. Shaffer, M. D. Powell, and J. Chen (1999), Comparisons of HRD and SLOSH surface wind fields in hurricanes: Implications for storm surge modeling, *Weather Forecast*, *14*(5), 671–686, doi:10.1175/1520-0434(1999)014.

Huang, Y., R. H. Weisberg, and L. Zheng (2010), Coupling of surge and waves for an Ivan-like hurricane impacting the Tampa Bay, Florida region, *J. Geophys. Res.*, *115*, C12009, doi:10.1029/2009JC006090.

Hubbard, M. E. (1999), Multidimensional slope limiters for MUSCL type finite volume schemes on unstructured grids, *J. Comput. Phys.*, *155*, 54–74.

Jarosz, E., D. A. Mitchell, D. W. Wang, and W. J. Teague (2007), Bottom-up determination of air-sea momentum exchange under a major tropical cyclone, *Science*, *315*(23), 1707–1709.

Jelesnianski, C. P. (1966), Numerical computations of storm surges without bottom stress, *Mon. Weather Rev.*, *94*, 279–394, doi:10.1175/1520-0493(1967)095.

Kees, W., R. Elmer, and J. van der Neut (2011), Improved surface-wave retrieval from ambient seismic noise by multi-dimensional deconvolution, *Geophys. Res. Lett.*, *38*, L01313, doi:10.1029/2010GL045523.

Kobayashi, M. H., J. M. C. Pereira, and J. C. F. Pereira (1999), A conservative finite-volume second-order-accurate projection method on hybrid unstructured grids, *J. Comput. Phys.*, *150*, 40–45.

Large, W. G., and S. Pond (1981), Open ocean momentum fluxes in moderate to strong winds, *J. Phys. Oceanogr.*, *11*, 324–336.

Mayfield, M. (1992), *Hurricane Bob Preliminary Report*, p. 4, National Hurricane Center, Miami, Fla.

McCoy A., J. W. Larry, and C. George (2008), Numerical investigation of flow hydrodynamics in a channel with a series of groynes, *J. Hydraul. Eng.*, *134*(2), 157–172, doi:10.1061/(ASCE)0733–9429(2008)134:2(157).

Mellor, G. L., and T. Yamada (1982), Development of a turbulence closure model for geophysical fluid problem, *Rev. Geophys. Space Phys.*, *20*, 851–875, doi:10.1029/RG020i004p00851.

Morton, R. A., R. G. James, and N. L. Scott (2008), Hydrodynamic implications of textural trends in sand deposits of the 2004 tsunami in Sri Lanka, *Sediment. Geol.*, *207*, 56–64, doi:10.1016/j.sedgeo.2008.03.008.

Orton, P., N. Georgas, A. Blumberg, and J. Pullen (2012), Detailed modeling of recent severe storm tides in estuaries of the New York City region, *J. Geophys. Res.*, *117*, C09030, doi:10.1029/2012JC008220.

Pasch, R., and L. Avila (1992), Atlantic hurricane season of 1991, *Mon. Weather Rev.*, *120*, 2671–2687.

Phadke, A. C., C. D. Martino, K. F. Cheung, and S. H. Houston (2003), Modeling of tropical cyclone winds and waves for emergency management, *Ocean Eng.*, *30*(4), 553–578, doi:10.1016/S0029-8018(02)00033-1.

Powell, M. D., and P. G. Black (1990), The relationship of hurricane reconnaissance flight-level measurements to winds measured by NOAA's oceanic platforms, *J. Wind Eng. Ind. Aerodyn.*, *36*(1-3), 381–392.

Powell, M. D., P. J. Vickery, and T. A. Reinhold (2003), Reduced drag coefficient for high wind speeds in tropical cyclones, *Nature*, *422*, 279–283.

Qi, J., C. Chen, R. C. Beardsley, W. Perrie, G. W. Cowles, and Z. Lai (2009), An unstructured-grid finite-volume surface wave model (FVCOM-SWAVE): Implementation, validations and applications, *Ocean Model.*, *28*, 153–166, doi:10.1016/j.ocemod.2009.01.007.

Rego, J. L., and C. Li (2010a), Storm surge propagation in Galveston Bay during Hurricane Ike, *J. Mar. Syst.*, *82*, 265–279, doi:10.1016/j.jmarsys.2010.06.001.

Rego, J. L., and C. Li (2010b), Nonlinear terms in storm surge predictions: Effect of tide and shelf geometry with case study from Hurricane Rita, *J. Geophys. Res.*, *115*, C06020, doi:10.1029/2009JC005285.

Skamarock, W. C., and J. B. Klemp (2008), A time-split nonhydrostatic atmospheric model for research and NWP applications, *J. Comput. Phys.*, *227*, 3465–3485.

Smagorinsky, J. (1963), General circulation experiments with the primitive equations, *Mon. Weather Rev.*, *91*, 99–164, doi:10.1175/1520-0493(1963)091.

SWAN Team (2006a), *SWAN Cycle III version 40.51 Technical documentation*, Fac. of Civil Eng. and Geosci., Environ. Fluid Mechanics Section, Delft Univ. of Technol., GA Delft, Netherlands.

SWAN Team (2006b), *SWAN Cycle III version 40.51 user manual*, Fac. of Civil Eng. and Geosci., Environ. Fluid Mechanics Section, Delft Univ. of Technol., GA Delft, Netherlands.

Ullman, D. S., and D. L. Codiga (2004), Seasonal variation of a coastal jet in the Long Island sound outflow region based on HF radar and Doppler current observations, *J. Geophys. Res.*, *109*, C07S06, doi:10.1029/2002JC001660.

Vickery, P. J., P. F. Sekerlj, and L. A. Twisdale (2000), Simulation of hurricane risk in the U.S. using empirical track model, *J. Struct. Eng.*, *126*(10), 1222–1237.

Warner, J. C., S. R. Christopher, and S. P. Richard (2008), Development of a three-dimensional, regional, coupled wave, current, and sediment-transport model, *Comput. Geosci.*, *34*, 1284–1306, doi:10.1016/j.cageo.2008.02.012.

Weisberg, R. H., and L. Zheng (2006), Hurricane storm surge simulations for Tampa Bay, *Estuarine Coast.*, *29*(6A), 899–913.

Weisberg, R. H., and L. Zheng (2008), Hurricane storm surge simulations comparing three-dimensional with two-dimensional formulations based on an Ivan-like storm over the Tampa Bay, Florida region, *J. Geophys. Res.*, *113*, C12001, doi:10.1029/2008JC005115.

Westerink, J. J., R. A. Luettich, J. C. Feyen, J. H. Atkinson, C. Dawson, H. J. Roberts, M. D. Powell, J. P. Dunion, E. J. Kubatko, and H. Pourtaheri (2008), A basin to channel scale unstructured grid hurricane storm surge model applied to southern Louisiana, *Mon. Weather Rev.*, *136*, 833–864, doi:10.1175/2007MWR1946.1.

Wu, L, C. Chen, F. Guo, M. Shi, J. Qi, and J. Ge (2010), A FVCOM-based unstructured grid wave, current, sediment transport model, I. model description and validation, *J. Ocean. Univ. China*, *10*, 1–8, doi:10.1007/s11802-011-1788-3.